Nonspecific activities of the major herbicide-resistance gene BAR

Authors: Bastien Christ[1], Ramon Hochstrasser[2]†, Luzia Guyer[2], Rita Francisco[2],
Sylvain Aubry[2], Stefan Hörtensteiner[2]* and Jing-Ke Weng[1,3]*

[1] Whitehead Institute for Biomedical Research, 455 Main Street, Cambridge, MA 02142-1479, USA.

[2] Department of Plant and Microbial Biology, University of Zurich, Zollikerstrasse 107, CH-8008 Zurich, Switzerland.

[3] Department of Biology, Massachusetts Institute of Technology, Cambridge, MA 02139, USA.

*Correspondence to. Email: shorten@botinst.uzh.ch (S.H.); wengj@wi.mit.edu (J.K.W.)

† Present address: Institute of Medical Microbiology, University of Zurich, Gloriastrasse 30/32, CH-8006, Zurich, Switzerland

**Bialaphos resistance (BAR) and phosphinothricin acetyltransferase (PAT)
genes, which convey resistance to the broad-spectrum herbicide phosphinothricin
(also known as glufosinate) via N-acetylation, have been globally used in basic plant
research and genetically engineered crops[1-4]. Although early in vitro enzyme assays
showed that recombinant BAR and PAT exhibit substrate preference toward
phosphinothricin over the 20 proteinogenic amino acids[1], indirect effects of BAR-
containing transgenes *in planta*, including modified amino acid levels, have been
seen but without the identification of their direct causes[5,6]. Combining
metabolomics, plant genetics, and biochemical approaches, we show that transgenic
BAR indeed converts two plant endogenous amino acids, aminoadipate and
tryptophan, to their respective N-acetylated products in several plant species
examined. We report the crystal structures of BAR, and further delineate structural
basis for its substrate selectivity and catalytic mechanism. Through structure-
guided protein engineering, we generated several BAR variants that display
significantly reduced nonspecific activities compared to its wild-type counterpart *in
vivo*. Our results demonstrate that transgenic expression of enzymes can result in
unintended off-target metabolism arising from enzyme promiscuity. Understanding
of such phenomena at the mechanistic level can facilitate the design of maximally
insulated systems featuring heterologously expressed enzymes.**

Phosphinothricin is a naturally occurring herbicide derived from the tripeptide
antibiotic bialaphos produced by species of *Streptomyces* soil bacteria. Phosphinothricin
is a structural analog of glutamate, and thereby inhibits glutamine synthetase, an essential
enzyme for glutamine synthesis and ammonia detoxification in plants, giving rise to its

37 herbicidal activity[3]. In the 1980s, the bialaphos resistance (*BAR*) gene and its closely

38 related homolog phosphinothricin acetyltransferase (*PAT*) gene were isolated from

39 *Streptomyces hygroscopicus* and *Streptomyces viridochromogenes*, respectively, and

40 were later broadly used as transgenes to confer herbicide resistance in a variety of major

41 genetically-engineered (GE) crops, including corn, soybean, canola, and cotton[7]. In

42 addition, *BAR* and *PAT* have also gained much utility in basic research as selection

43 markers for generating transgenic plants[1]. Despite the prevalent use of *BAR* and *PAT* in

44 the context of generating herbicide-resistant transgenic plants, whether these bacteria-

45 derived enzymes may possibly interfere with plant endogenous metabolism has not been

46 rigorously investigated.

47 In research not initially intended to address this issue regarding phosphinothricin-

48 resistance trait, we carried out untargeted metabolomics analysis on senescent leaf

49 extracts prepared from the *Arabidopsis thaliana clh2-1* mutant (FLAG_76H05, referred

50 to as FLAG-1 hereafter), which contains a transfer DNA (T-DNA) insertion that

51 abolishes the *CHLOROPHYLLASE 2* gene[8]. This analysis revealed two metabolites that

52 were ectopically accumulated at high levels in *clh2-1* compared to wild type (Fig. 1a).

53 Using liquid chromatography-tandem mass spectrometry (LC-MS[2]), we identified these

54 two metabolites as N-acetyl-aminoadipate and N-acetyl-tryptophan (referred to as acetyl-

55 aminoadipate and acetyl-tryptophan, respectively, hereafter; Fig. 1a and Supplementary

56 Fig. 1). Because the deficiency of CHLOROPHYLLASE 2, a serine esterase[8], in *clh2-1*

57 does not explain the accumulation of these acetylated metabolites, we hypothesized that

58 the *BAR* gene present on the T-DNA as a selection marker in *clh2-1* might be responsible

59 for their formation. To test this, we extended our metabolomics analysis to additional

60 Arabidopsis T-DNA insertional mutants unrelated to chlorophyll metabolism that carry

61 either *BAR* (e.g. mutants from the FLAG[9] and SAIL[10] collections) or alternative antibiotic

62 selection markers (e.g. mutants from the SALK (*NTPII*, kanamycin resistance)[11] and

63 GABI (*SULI*, sulfadiazine resistance)[12] collections (Supplementary Table 1). Senescent

64 leaves of all six T-DNA mutants carrying *BAR* manifested accumulation of acetyl-

65 aminoadipate and acetyl-tryptophan, while these metabolites were significantly lower or

66 not detected in wild-type plants and T-DNA mutants containing alternative selection

67 markers (Fig. 1b). These results indicate that the ectopic accumulation of these

68 metabolites is likely resulted from the nonspecific N-acetyltransferase activities of

69 transgenic BAR acting upon plant endogenous amino acids.

70   We quantified the absolute concentrations of acetyl-aminoadipate and acetyl-

71 tryptophan in senescent leaves of *BAR*-containing transgenic Arabidopsis to range from

72 306 to 845 nmole/g and from 14 to 76 nmole/g fresh weight, respectively (Supplementary

73 Fig. 2). While trace level of acetyl-tryptophan can be detected in wild-type Arabidopsis,

74 acetyl-aminoadipate was undetectable in wild-type samples (Supplementary Fig. 2). The

75 ectopic accumulation of acetyl-aminoadipate and acetyl-tryptophan in *BAR*-containing

76 transgenic Arabidopsis is substantial given that the concentrations of free aminoadipate

77 and tryptophan in senescent leaves of these Arabidopsis lines are in the ranges of 61 to

78 122 nmole/g and from 1566 to 2663 nmole/g fresh weight, respectively (Supplementary

79 Fig. 2). On the other hand, the concentrations of free amino acids in senescent leaves do

80 not seem to be significantly affected by the expression of BAR, as revealed by the

81 quantification of 21 other amino acids (Supplementary Fig. 2).

82   To assess whether the nonspecific activities of transgenic BAR also manifest in

83   other plant hosts, we performed metabolic profiling of various tissue samples from

84   phosphinothricin-resistant soybean (*Glycine max*), canola (*Brassica napus*), mustard

85   (*Brassica juncea*) and wheat (*Triticum aestivum*). Substantially increased accumulation

86   of acetyl-aminoadipate and acetyl-tryptophan was also detected in some tissues of these

87   transgenic lines (Supplementary Fig. 3), indicating that our findings regarding the *in vivo*

88   nonspecific activities of BAR may apply broadly to a wide range of *BAR*-containing

89   transgenic plants.

90   The concentration of free tryptophan is low in photosynthetically active leaves,

91   but increases significantly in senescent leaves[13]. This is due to enhanced proteolysis

92   during senescence, facilitating remobilization of protein-bound nitrogen and other

93   nutrients to sink organs, such as seeds[14]. Aminoadipate, an intermediate of lysine

94   degradation, also exhibits a similar accumulation pattern during leaf senescence[15]. To test

95   whether the BAR-catalyzed production of acetyl-aminoadipate depends on lysine

96   degradation, we analyzed an Arabidopsis mutant from the FLAG collection,

97   FLAG_*lkrsdh*, in which the *BAR*-containing T-DNA disrupts *At4g33150* encoding the

98   Arabidopsis bifunctional lysine-ketoglutarate reductase/saccharopine dehydrogenase

99   (LKR/SDH, Supplementary Fig. 4)[16]. LKR/SDH catalyzes the first committed step of

100   lysine degradation, and, together with the subsequent aminoadipate semialdehyde

101   dehydrogenase (AADH), converts lysine to aminoadipate (Fig. 2a). In a segregating

102   population for the FLAG_*lkrsdh* locus, heterozygous, homozygous and wild-type plants

103   were identified by genotyping, and subjected to LC-MS metabolic profiling after

104   senescence induction (Fig. 2b, Supplementary Fig. 4). Acetyl-aminoadipate occurred at

105 the highest level in the heterozygous mutant, but was greatly reduced in the homozygous

106 mutant, suggesting that the ectopic accumulation of acetyl-aminoadipate in *BAR*-

107 containing plants is dependent on the activity of LKR/SDH in the lysine degradation

108 pathway in senescent leaves (Fig. 2a). By contrast, the relative abundance of acetyl-

109 tryptophan in the segregating population of FLAG_*lkrsdh* generally reflected the copy

110 number of the *BAR*-containing T-DNA transgene, with approximately 2-fold acetyl-

111 tryptophan level observed in the homozygotes compared to the heterozygotes (Fig. 2b).

112 Furthermore, acetyl-aminoadipate and acetyl-tryptophan levels were approximately 10-20

113 fold higher in senescent leaves than those in green leaves (Fig. 2b), which is likely due to

114 the increased availability of the corresponding free amino acids during senescence.

115 Consistent with these observations in leaves, ectopic accumulation of acetyl-

116 aminoadipate and acetyl-tryptophan was also observed in seeds of multiple *BAR*-

117 containing T-DNA mutant lines compared to the wild-type controls (Supplementary Fig.

118 5).

119   To shed light on the kinetic properties of BAR, we carried out pseudo-first-order

120 enzyme kinetic assays using recombinant BAR against several native and non-native

121 amino acid substrates (Fig. 3 and Supplementary Fig. 6). Similar to published data[1,3,17],

122 N-acetylation of phosphinothricin exhibits Michaelis-Menten kinetics with an apparent

123 K_m of approximately 132 µM (Fig. 3). Although BAR clearly showed N-acetyltransferase

124 activities toward aminoadipate and tryptophan, K_m values for these non-native substrates

125 could not be established, as both substrates reached solubility limit before reaching

126 saturation concentration for BAR. V_{max}/K_m values of BAR against aminoadipate and

127 tryptophan, which were inferred from Lineweaver-Burk plots, reveals that these two side

128 reactions are less favorable than the acetylation of phosphinothricin. BAR also exhibited

129 relatively higher catalytic activity toward aminoadipate than tryptophan *in vitro* (Fig. 3).

130   To reveal the structural basis for substrate selectivity and catalytic mechanism of

131 BAR that would enable structure-guided protein engineering, we determined the crystal

132 structures of the BAR/acetyl-CoA holocomplex and the BAR/CoA/phosphinothricin

133 ternary complex (see Supplementary Table 2 for data collection and refinement

134 statistics). Our refined structures revealed that BAR is an αβ protein harboring a globular

135 tertiary structure resembling the previously reported Gcn5-related N-acetyltransferase

136 (GNAT) structures (Supplementary Fig. 7)[18-21]. BAR crystalizes as a homodimer with

137 two active sites symmetrically distributed around the dimer interface inside a large open

138 cavity (Fig. 4a and Supplementary Fig. 8). The cofactor acetyl-CoA binds to a cleft

139 between α4 and α5 on the opposite side of the dimer interface with the acetyl group

140 pointing toward the catalytic center (Fig. 4a). Close examination of the BAR/acetyl-CoA

141 and BAR/CoA/phosphinothricin structures illuminates the catalytic mechanism of BAR

142 (Fig. 4b, 4c and Supplementary Fig. 9). Similar to other GNATs, BAR utilizes a

143 conserved catalytic Glu88 as a general base to deprotonate the amino group of

144 phosphinothricin through a water molecule as the proton shuttle (Fig. 4b, 4c, and

145 Supplementary Fig. 9)[21]. The deprotonated amino group then undergoes nucleophilic

146 attack on the carbonyl carbon of acetyl-CoA to produce a tetrahedral intermediate, which

147 is further stabilized by an oxyanion hole formed by a positively charged H137 and its

148 proton donor Y107 (Fig. 4c and Supplementary Fig. 9). Interestingly, the structural

149 feature underlying this oxyanion hole in BAR must have arisen independently from the

150 functionally   analogous   oxyanion   hole   previously   described   in   the   histone

151 acetyltransferase GCN5, featuring a backbone amide nitrogen instead[21]. In the final step

152 of the catalytic cycle, coenzyme A is released from the tetrahedral intermediate as a

153 leaving group to produce acetyl-phosphinothricin (Fig. 4c).

154   The BAR/CoA/phosphinothricin ternary structure also reveals active-site residues

155 involved in phosphinothricin binding. Within each active site, the methylphosphoryl

156 group of the substrate engages hydrophobic interactions with the surrounding F36, G127,

157 and V161 from the same monomer, whereas the two phosphoryl oxygen atoms are

158 coordinated by K78, R80, and Y83 from the β3-loop-α3 region of the neighboring

159 monomer via a set of hydrogen bonds and electrostatic interactions (Fig. 4b).

160 Furthermore, the amino acid group of phosphinothricin is properly positioned at the

161 catalytic center by a hydrogen-bond network involving the backbone carbonyl group of

162 V125 and the side chains of T90 and Y92 (Fig. 4b). Despite various attempts using co-

163 crystallization and soaking techniques, structures of BAR containing aminoadipate or

164 tryptophan could not be obtained, reflecting the low affinity of these nonspecific

165 substrates to BAR. Simulated docking of these substrates within the active site of the

166 BAR/CoA/phosphinothricin structure reveals fewer favorable interactions as well as

167 potential steric clashes with the surrounding residues compared to phosphinothricin (Fig.

168 4d).

169   Site-directed mutagenesis followed by biochemical assays confirmed the roles of

170 many active-site residues predicted by structural analysis (Fig. 4e and Supplementary

171 Fig. 10). Mutating the catalytic E88 to alanine or glutamine greatly reduces the activity of

172 BAR toward phosphinothricin and aminoadipate. Nevertheless, these mutants exhibit

173 higher activity toward tryptophan than that of the wild-type enzyme at the substrate

174   concentration tested (Fig. 4e), suggesting that tryptophan may be deprotonated through

175   an alternative mechanism independent of E88 and/or the first deprotonation step is not

176   rate-limiting for BAR-catalyzed acetyl-tryptophan formation. H137A and Y107F mutants

177   failed to yield sufficient soluble recombinant protein (Supplementary Fig. 10), preventing

178   the role of the oxyanion hole in catalysis to be directly assessed. We thus probed this

179   indirectly by mutating S133, a residue that forms a hydrogen bond with the imidazole

180   ring π-nitrogen of H137 (Fig. 4b). The resulting S133A mutant exhibits completely

181   abolished N-acetyltransferase activity toward the three tested substrates, suggesting an

182   essential role of S133 in catalysis, likely through proper positioning of the imidazoline

183   ring of the histidine within the oxyanion hole (Fig. 4e and Supplementary Fig. 9).

184   Mutants affecting phosphinothricin-binding residues, including F36A, K78A, R80A,

185   Y83F, Y92F, generally show significantly reduced activity toward phosphinothricin and

186   aminoadipate, while K78A and Y83F display increased activity toward the more

187   hydrophobic substrate tryptophan compared to the wild-type enzyme (Fig. 4e).

188   With the structural information of BAR in hand, we sought to engineer BAR

189   through structure-guided mutagenesis to repress its undesired nonspecific activities

190   toward aminoadipate and tryptophan while maintaining its native activity against

191   phosphinothricin. We selected residue positions N35, Y73, T90, Y92, and V125 for

192   targeted mutagenesis based on structural analysis as well as multiple sequence alignment

193   containing BAR, PAT, and other closely related homologs from bacteria (Fig. 4b, 4d and

194   Supplementary Fig. 11). A set of eleven mutants was first characterized *in vitro* (Fig. 4e),

195   and eight of them were further tested in transgenic Arabidopsis (Fig. 4f and 4g). All eight

196   BAR mutants confer phosphinothricin resistance in Arabidopsis T1 and T2 generations

197   (Fig. 4f, Supplementary Fig. 12-14). Metabolic profiling of these transgenic lines

198   confirmed that mutations in select active-site residues of BAR can modulate the *in vivo*

199   nonspecific activities of BAR toward aminoadipate and tryptophan (Fig. 4g). Notably,

200   transgenic Arabidopsis plants containing Y73F, Y92F, N35T, N35D, T90A, V125L, or

201   V125I BAR mutants display significantly reduced levels of acetyl-aminoadipate

202   compared to plants containing wild-type BAR (Fig. 4g). Moreover, plants expressing

203   Y73F, Y92F or T90A BAR mutants exhibit significantly reduced levels of both acetyl-

204   aminoadipate and acetyl-tryptophan compared to plants containing wild-type BAR. These

205   observed differences in acetyl-aminoadipate and acetyl-tryptophan levels are not due to

206   BAR protein levels in transgenic plants (Supplementary Fig. 15), but are consistent with

207   the altered catalytic activities of various BAR mutants measured *in vitro* (Fig. 4e and

208   Supplementary Fig. 16). Subsequent analysis of N35T and Y92F revealed that both

209   mutants exhibit compromised affinity toward native substrate phosphinothricin *in vitro*

210   compared to wild-type BAR. However, N35T and Y92F retain largely unaltered catalytic

211   speed *in vitro* and confer level of resistance to phosphinothricin *in planta* similar to that

212   of wild-type BAR (Supplementary Fig. 16a and Supplementary Fig. 14). Furthermore,

213   both mutants show more pronounced reduced catalytic activity toward one or both non-

214   native substrates as compared to phosphinothricin (Supplementary Fig. 16).

215   Transgenic expression of enzymes catalyzing a variety of desirable biochemical

216   reactions in heterologous hosts is a common strategy in both basic biological research

217   and translational biotechnology. Prominent examples include reporter enzymes, such as

218   firefly luciferase and β-glucuronidase, antibiotic/herbicide markers, such as

219   aminoglycoside kinase that confers kanamycin resistance and BAR, and many enzymes

10

220   used for metabolic engineering purposes in microbes and higher eukaryotes[22]. Although

221   enzymes are generally considered as perfected catalysts with superior substrate

222   specificity and predictable catalytic mechanism, increasing evidences have raised

223   awareness of the unpredictable behaviors of enzymes and their profound implication in

224   natural and directed evolution of new enzymatic functions[23]. However, whether and how

225   heterologous expression of a foreign enzyme would interfere with the native metabolic

226   system remains an open question to be addressed on a case-by-case basis.

227   In this study, we discovered that transgenic expression of the herbicide-resistance

228   enzyme BAR of bacterial origin indeed acetylate two endogenous amino acids, resulting

229   in the ectopic accumulation of acetyl-aminoadipate and acetyl-tryptophan. While acetyl-

230   tryptophan is a naturally occurring metabolite found in numerous plant species, including

231   Arabidopsis, *Salsola collina*, *Glycine max*, *Solanum lycopersicum*, *Cocos nucifera*, and

232   *Ginkgo biloba*[24,25], to the best of our knowledge, acetyl-aminoadipate has never been

233   reported as an endogenous plant metabolite. Interestingly, in line with our findings, a

234   recent study reported the ectopic accumulation of acetyl-aminoadipate in the flower

235   tissue of a BAR-containing T-DNA mutant of Arabidopsis, which could not be

236   rationalized by the mutated gene[26]. Despite the widespread use of BAR in GE crops[2,27]

237   and the extensive testing and deregulation processes associated with this trait over the

238   past few decades[1,3,17,28,29], such phenomenon was not reported elsewhere, probably due to

239   technological limitation in metabolic profiling in the past. Studies have demonstrated

240   indirect effects of BAR-containing transgenes in transgenic lines with high BAR

241   expression, such as reduced fitness and modified amino acid levels, but without

242   identifying their direct causes[5,6]. However, the implications of our findings about the

243 nonspecific activities of BAR on crop fitness and human/animal health are yet to be

244 evaluated in future studies.

245   Our findings suggest that untargeted metabolomics analysis could be a useful

246 methodology for future assessment of GE plants[7]. This study also provides solutions to

247 reduce the nonspecific activities of BAR through structure-guided enzyme engineering so

248 that its intended herbicide-degrading activity can be maximally insulated from the

249 metabolome of the host.

250

251 CORRESPONDING AUTHORS

252 Correspondence to Jing-Ke Weng or Stefan Hörtensteiner.

253

271   AUTHOR CONTRIBUTIONS

272   B.C., S.A., S.H. and J.K.W. designed experiments; B.C., R.H., L.G., R.F. and S.A.

273   performed experiments; B.C., R.H., L.G. and J.K.W. analyzed data; B.C., S.H., S.A. and

274   J.K.W. wrote the manuscript.

275

276   COMPETING FINANCIAL INTERESTS

277   B.C. and J.K.W. have filed a patent application on BAR and PAT mutants described in

278   this paper that show altered acetyltransferase activity.

279

280

281   REFERENCES

282   1   Wehrmann, A., Van Vliet, A., Opsomer, C., Botterman, J. & Schulz, A. The similarities of *BAR*
283   and *PAT* gene products make them equally applicable for plant engineers. *Nat. Biotechnol.* **14**,
284   1274-1278 (1996).
285   2   Duke, S. O. Taking stock of herbicide-resistant crops ten years after introduction. *Pest. Manag.*
286   *Sci.* **61**, 211-218 (2005).
287   3   Thompson, C. J. *et al.* Characterization of the herbicide-resistance gene *BAR* from *Streptomyces*
288   *hygroscopicus*. *EMBO J.* **6**, 2519-2523 (1987).
289   4   Wohlleben, W. *et al.* Nucleotide sequence of the phosphinothricin N-acetyltransferase gene from
290   *Streptomyces viridochromogenes* Tü494 and its expression in *Nicotiana tabacum*. *Gene* **70**, 25-37
291   (1988).
292   5   Ren, Y. F. *et al.* A comparative proteomics approach to detect unintended effects in transgenic
293   Arabidopsis. *J. Genet. Genomics* **36**, 629-639 (2009).
294   6   Brown, R. H., Raboy, V. & Bregitzer, P. Unintended consequences: high phosphinothricin
295   acetyltransferase activity related to reduced fitness in barley. *In Vitro Cell. Dev. Biol. Plant* **49**,
296   240-247 (2013).
297   7   The National Academies. *Genetically Engineered Crops: Experiences and Prospects.* (National
298   Academies Press, 2016).
299   8   Schenk, N. *et al.* The chlorophyllases *At*CLH1 and *At*CLH2 are not essential for senescence-
300   related chlorophyll breakdown in *Arabidopsis thaliana*. *FEBS Lett.* **581**, 5517-5525 (2007).
301   9   Samson, F. *et al.* FLAGdb/FST: a database of mapped flanking insertion sites (FSTs) of
302   *Arabidopsis thaliana* T-DNA transformants. *Nucleic Acids Res.* **30**, 94-97 (2002).
303   10   Sessions, A. *et al.* A high-throughput Arabidopsis reverse genetics system. *Plant Cell* **14**, 2985-
304   2994 (2002).
305   11   Alonso, J. M. *et al.* Genome-wide insertional mutagenesis of *Arabidopsis thaliana*. *Science* **301**,
306   653-657 (2003).
307   12   Rosso, M. G. *et al.* An *Arabidopsis thaliana* T-DNA mutagenized population (GABI-Kat) for
308   flanking sequence tag-based reverse genetics. *Plant Mol. Biol.* **53**, 247-259 (2003).
309   13   Soudry, E., Ulitzur, S. & Gepstein, S. Accumulation and remobilization of amino acids during
310   senescence of detached and attached leaves: *in planta* analysis of tryptophan levels by
311   recombinant luminescent bacteria. *J. Exp. Bot.* **56**, 695-702 (2005).
312   14   Hörtensteiner, S. & Feller, U. Nitrogen metabolism and remobilization during senescence. *J. Exp.*
313   *Bot.* **53**, 927-937 (2002).
314   15   Arruda, P., Kemper, E. L., Papes, F. & Leite, A. Regulation of lysine catabolism in higher plants.
315   *Trends Plant Sci.* **5**, 324-330 (2000).
316   16   Zhu, X., Tang, G., Granier, F., Bouchez, D. & Galili, G. A T-DNA insertion knockout of the
317   bifunctional *LYSINE-KETOGLUTARATE REDUCTASE/SACCHAROPINE DEHYDROGENASE*
318   gene elevates lysine levels in Arabidopsis seeds. *Plant Physiol.* **126**, 1539-1545 (2001).
319   17   Vinnemeier, J., DrogeLaser, W., Pistorius, E. K. & Broer, I. Purification and partial
320   characterization of the *Streptomyces viridochromogenes* Tü494 phosphinothricin-N-
321   acetyltransferase mediating resistance to the herbicide phosphinothricin in transgenic plants. *Z.*
322   *Naturforsch. C.* **50**, 796-805 (1995).
323   18   Dyda, F., Klein, D. C. & Hickman, A. B. GCN5-related N-acetyltransferases: a structural
324   overview. *Annu. Rev. Bioph. Biom.* **29**, 81-103 (2000).
325   19   Vetting, M. W. *et al.* Structure and functions of the GNAT superfamily of acetyltransferases.
326   *Arch. Biochem. Biophys.* **433**, 212-226 (2005).
327   20   Srivastava, P. *et al.* Structural characterization of a GCN5-related N-acetyltransferase from
328   *Staphylococcus aureus*. *PLoS ONE* **9** (2014).
329   21   Rojas, J. R. *et al.* Structure of Tetrahymena GCN5 bound to coenzyme A and a histone H3
330   peptide. *Nature* **401**, 93-98 (1999).
331   22   Woolston, B. M., Edgar, S. & Stephanopoulos, G. Metabolic engineering: past and future. *Annu.*
332   *Rev. Chem. Biomol. Eng.* **4**, 259-288 (2013).
333   23   Weng, J. K. & Noel, J. P. The remarkable pliability and promiscuity of specialized metabolism.
334   *Cold Spring Harb. Symp. Quant. Biol.* **77**, 309-320 (2012).

335 24 Jin, Y.-S. *et al.* Chemical and biologically active constituents of *Salsola collina. Chem. Nat.*
336   *Compd.* **47**, 257-260 (2011).
337 25 Yu, P., Hegeman, A. D. & Cohen, J. D. A facile means for the identification of indolic compounds
338   from plant tissues. *Plant J.* **79**, 1065-1075 (2014).
339 26 Bruckhoff, V. *et al.* Functional characterization of CYP94-genes and identification of a novel
340   jasmonate catabolite in flowers. *PLoS One* **11**, e0159875 (2016).
341 27 Green, J. M. & Owen, M. D. Herbicide-resistant crops: utilities and limitations for herbicide-
342   resistant weed management. *J. Agric. Food Chem.* **59**, 5819-5829 (2011).
343 28 Herouet, C. *et al.* Safety evaluation of the phosphinothricin acetyltransferase proteins encoded by
344   the *PAT* and *BAR* sequences that confer tolerance to glufosinate-ammonium herbicide in
345   transgenic plants. *Regul. Toxicol. Pharm.* **41**, 134-149 (2005).
346 29 Dan, Y. *Plant transformation technology revolution in last three decades: historical technology*
347   *developments*. (Bentham Science Publishers, 2012).
348 30 Song, W. Y., Choi, K. S., Alexis de, A., Martinoia, E. & Lee, Y. Brassica juncea plant cadmium
349   resistance 1 protein (BjPCR1) facilitates the radial transport of calcium in the root. *Proc. Natl.*
350   *Acad. Sci. U.S.A.* **108**, 19808-19813 (2011).
351 31 Foetzki, A. *et al.* Surveying of pollen-mediated crop-to-crop gene flow from a wheat field trial as
352   a biosafety measure. *GM Crops Food* **3**, 115-122 (2012).
353 32 Czechowski, T., Stitt, M., Altmann, T., Udvardi, M. K. & Scheible, W. R. Genome-wide
354   identification and testing of superior reference genes for transcript normalization in Arabidopsis.
355   *Plant Physiol.* **139**, 5-17 (2005).
356 33 Chambers, M. C. *et al.* A cross-platform toolkit for mass spectrometry and proteomics. *Nat.*
357   *Biotechnol.* **30**, 918-920 (2012).
358 34 Gowda, H. *et al.* Interactive XCMS Online: simplifying advanced metabolomic data processing
359   and subsequent statistical analyses. *Anal. Chem.* **86**, 6931-6939 (2014).
360 35 Smith, C. A. *et al.* METLIN: a metabolite mass spectral database. *Ther. Drug Monit.* **27**, 747-751
361   (2005).
362 36 Tropea, J. E., Cherry, S. & Waugh, D. S. Expression and purification of soluble His(6)-tagged
363   TEV protease. *Methods Mol. Biol.* **498**, 297-307 (2009).
364 37 Battye, T. G., Kontogiannis, L., Johnson, O., Powell, H. R. & Leslie, A. G. iMOSFLM: a new
365   graphical interface for diffraction-image processing with MOSFLM. *Acta Crystallogr. D* **67**, 271-
366   281 (2011).
367 38 Evans, P. Scaling and assessment of data quality. *Acta Crystallogr. D* **62**, 72-82 (2006).
368 39 Adams, P. D. *et al.* PHENIX: a comprehensive Python-based system for macromolecular structure
369   solution. *Acta Crystallogr. D* **66**, 213-221 (2010).
370 40 Emsley, P. & Cowtan, K. Coot: model-building tools for molecular graphics. *Acta Crystallogr. D*
371   **60**, 2126-2132 (2004).
372 41 Goldstein, A. L. & McCusker, J. H. Three new dominant drug resistance cassettes for gene
373   disruption in *Saccharomyces cerevisiae. Yeast* **15**, 1541-1553 (1999).
374 42 Engler, C. *et al.* A Golden Gate modular cloning toolbox for plants. *ACS Synth. Biol.* (2014).
375 43 Clough, S. J. & Bent, A. F. Floral dip: a simplified method for Agrobacterium-mediated
376   transformation of *Arabidopsis thaliana. Plant J.* **16**, 735-743 (1998).
377 44 Schelbert, S. *et al.* Pheophytin pheophorbide hydrolase (pheophytinase) is involved in chlorophyll
378   breakdown during leaf senescence in Arabidopsis. *Plant Cell* **21**, 767-785 (2009).
379 45 Christ, B. *et al.* MES16, a member of the methylesterase protein family, specifically demethylates
380   fluorescent chlorophyll catabolites during chlorophyll breakdown in Arabidopsis. *Plant Physiol.*
381   **158**, 628-641 (2012).
382 46 Guyer, L. *Characterization of dephytylation and dechelation, two early steps of chlorophyll*
383   *breakdown in leaves and fruits* PhD thesis, Zurich, (2015).
384 47 Christ, B. *et al.* Cytochrome P450 CYP89A9 is involved in the formation of major chlorophyll
385   catabolites during leaf senescence in Arabidopsis. *Plant Cell* **25**, 1868-1880 (2013).
386 48 Perez-Perez, J. M. *et al.* Functional redundancy and divergence within the Arabidopsis
387   RETICULATA-RELATED gene family. *Plant Physiol.* **162**, 589-603 (2013).
388 49 Christ, B. *Chlorophyll breakdown: modifications of colorless chlorophyll catabolites* PhD thesis,
389   Zurich, (2013).

390   50   Zufferey, M. *et al.* The novel chloroplast outer membrane kinase KOC1 is a required component
391   of the plastid protein import machinery. *J. Biol. Chem.* **292**, 6952-6964 (2017).
392   51   Pulido, P., Llamas, E. & Rodriguez-Concepcion, M. Both Hsp70 chaperone and Clp protease
393   plastidial systems are required for protection against oxidative stress. *Plant Signal. Behav.* **12**
394   (2017).
395   52   Waterhouse, A. M., Procter, J. B., Martin, D. M., Clamp, M. & Barton, G. J. Jalview Version 2 - a
396   multiple sequence alignment editor and analysis workbench. *Bioinformatics* **25**, 1189-1191
397   (2009).

398

399   FIGURE LEGENDS

400   **Figure 1 | Accumulation of acetyl-aminoadipate and acetyl-tryptophan in senescent**

401   **leaves of Arabidopsis carrying the BAR transgene**. **a**, Metabolite profiles of senescent

402   leaves from Wassilewskija (Ws) and *clh2-1* (FLAG-1), displayed as base peak

403   chromatograms (BPC), reveal the ectopic accumulation of acetyl-aminoadipate (**1**) and

404   acetyl-tryptophan (**2**). BPC traces of four biological replicates are displayed. **b**,

405   Comparative levels of acetyl-aminoadipate and acetyl-tryptophan in Arabidopsis mutants

406   from different insertional mutant collections that contain either BAR (SAIL and FLAG)

407   or alternative selection marker genes (SALK (*NTPII*, kanamycin resistance) and GABI

408   (*SULI*, sulfadiazine resistance)). Error bars, mean ± s.d. (n = 3 biological replicates). This

409   experiment was repeated at least three times with similar results. See Supplementary Fig.

410   2 for absolute quantification. a.u., arbitrary unit; FW, fresh weight; n.d., not detected

411

412   **Figure 2 | BAR-dependent accumulation of acetyl-aminoadipate and acetyl-**

413   **tryptophan is linked to nitrogen remobilization during senescence**. **a**, Aminoadipate

414   is derived from the lysine degradation pathway in plants, which can be metabolized by

415   BAR as a nonspecific substrate. **b**, Comparative levels of acetyl-aminoadipate and acetyl-

416   tryptophan in green and senescent leaves from the heterozygous (He) and homozygous

417   (Ho) FLAG_*lkrsdh* mutant, harboring a BAR-containing T-DNA that abolishes the

17

418   Arabidopsis *LKR/SDH* gene. Error bars, mean ± s.d. (n = 4 biological replicates). a.u.,

419   arbitrary unit; n.d., not detected; Ws, Wassilewskija wild-type plants.

420

421   **Figure 3 | In vitro enzyme kinetic assays of BAR against native and non-native**

422   **substrates.** An apparent K_M value of 132 ± 19.2 µM was obtained for phosphinothricin,

423   similar to previously published data[1,3,17]. V_{max}, k_{cat}, k_{cat}/K_m and V_{max}/K_m values for

424   phosphinothricin are also indicated, as well V_{max}/K_m values for aminoadipate and

425   tryptophan (estimated from Lineweaver-Burk plots). Aminoadipate and tryptophan are in

426   vitro substrates of BAR but both substrates reached solubility limit before reaching

427   saturation concentration for BAR. Negative controls (open circles) were performed in

428   absence of BAR at the highest substrate concentration tested (20 mM).

429

430   **Figure 4 | Structural basis for amino acid N-acetylation catalyzed by BAR and**

431   **structure-guided engineering of BAR with reduced nonspecific activities. a**, Cartoon

432   representation of BAR homodimer in complex with phosphinothricin and CoA. Two

433   monomers of the dimer are colored in blue and yellow respectively. **b**, Close-up view of

434   the BAR active site. The |2Fo-Fc| omit electron density map (contoured at 3.0 σ) is

435   shown for phosphinothricin. **c**, Proposed catalytic mechanism of BAR. **d**, Docking of

436   tryptophan and aminoadipate within the BAR active site reveals reduced favorable

437   contacts compared to phosphinothricin. **e**, Enzyme activity assays using purified BAR

438   mutant proteins against phosphinothricin (0.2mM), aminoadipate (1 mM) and tryptophan

439   (1 mM). Wild-type BAR (WT BAR) and PAT from Streptomyces viridochromogenes

440   were also examined as controls. Assays were terminated during the initial linear rate of

441   product formation. The relative amount of product formed by each BAR mutant was

442   normalized to WT BAR for each substrate (value of 1). Error bars, mean ± s.d. (n = 3

443   technical replicates). **f**, Photographs of Arabidopsis T1 lines transformed with select BAR

444   mutants 10 days after phosphinothricin treatment (see also Supplementary Fig. 12-14).

445   Scale bar = 0.3 cm. **g**, Comparative levels of acetyl-aminoadipate and acetyl-tryptophan

446   in phosphinothricin-resistant T2 Arabidopsis plants transformed with selected BAR

447   mutants. Error bars, mean ± s.d. (n = 5-6 biological replicates: Y73F (6), Y92F (6), N35T

448   (5), N35S (5), T90A (6), V125T (5), V125L (6), V125I (6), WT BAR (5), PAT (5)).

449   Significance levels were indicated based on one-way ANOVA with Dunnett's test for

450   multiple comparisons to WT BAR. a, p-value < 0.1; b, p-value < 0.05; c, p-value < 0.01;

451   a.u., arbitrary unit.

452

453   **Materials and Methods**

454   **Plant materials**

455   Arabidopsis (*Arabidopsis thaliana*) Columbia-0 (Col-0) and Wassilewskija (Ws) were

456   used as wild types. T-DNA insertion lines were from the following collections: SALK

457   lines[11]: SALK_130606 (SALK_1), SALK_051823C (SALK_2), SALK_110649

458   (SALK_3); SAIL lines[10]: SAIL_1165_B02 (SAIL_1), SAIL_503_C03 (SAIL_2),

459   SAIL_1235_D10 (SAIL_3); GABI lines[12]: GABI_453E01 (GABI_1), GABI_833F02

460   (GABI_2), GABI_453A08 (GABI_3); FLAG lines[9]: FLAG_076H05 (*clh2-1*[8]; FLAG_1),

461   FLAG_271B02 (FLAG_2), FLAG_495A09 (FLAG_3), FLAG_271B12 (FLAG_*lkrsdh*).

462   SALK, SAIL and GABI lines were obtained from the European Arabidopsis Stock

463   Center (http://arabidopsis.info/). The FLAG lines were obtained from the INRA

464 Versailles Arabidopsis Stock Center (http://publiclines.versailles.inra.fr/). Homozygous

465 (and heterozygous for FLAG_*lkrsdh*) plants were identified by PCR using T-DNA- and

466 gene-specific primers.

467 Arabidopsis T-DNA lines used for untargeted metabolomics and relative

468 quantification of acetyl-aminoadipate and acetyl-tryptophan were grown on soil under a

469 12-h-light/12-h-dark photoperiod with fluorescent light of 80 to 120 μmol photons m^{-2} s^{-1}

470 at 22°C and 60% relative humidity. For senescence induction, leaves from 5-week-old

471 plants were excised and incubated in permanent darkness on wet filter paper for 8 d at

472 ambient temperature. Transgenic Arabidopsis lines transformed with BAR mutants and

473 Arabidopsis T-DNA lines used for absolute quantification of acetyl-aminoadipate and

474 acetyl-tryptophan were grown on soil under a 16-h-light/8-h-dark photoperiod with

475 fluorescent light of 80 to 120 μmol photons m^{-2} s^{-1} at 22°C and 60% relative humidity.

476 For senescence induction, leaves from phosphinothricin-resistant, 4-week-old plants were

477 excised and incubated in permanent darkness on wet filter paper for 6 d at ambient

478 temperature. For measuring the expression of LKR/SDH in FLAG_271B12, seedlings

479 were grown for 7 days on ½ Murashige and Skoog (MS) plates containing 1% sucrose.

480 Phosphinothricin-resistant *Glycine max* (Liberty Link trait A2704-12, 283 Morril

481 MC-116, Credenz CZ 3841 LL, Bayer CropScience), wild-type (non-isogenic) *Glycine*

482 *max* (Chiba Green; High Mowing Organic Seed), lines were grown on soil under a 16-h-

483 light/8-h-dark photoperiod with fluorescent light of 80 to 120 μmol photons m^{-2} s^{-1} at

484 22°C and 60% relative humidity. Green and senescent leaf samples were collected from

485 40-days old plants. This experiment was repeated once with similar results.

486   Phosphinothricin-resistant *Brassica napus* (Liberty Link trait L252, Bayer

487   CropScience) and wild-type (non-isogenic) *Brassica napus* (NDC-E12131, NDC-E13285

488   and NDC-E12027) lines were grown on soil under a 16-h-light/8-h-dark photoperiod with

489   fluorescent light of 80 to 120 μmol photons m^{-2} s^{-1} at 22°C and 60% relative humidity.

490   For senescence induction, fully developed cotyledons were excised and incubated in

491   permanent darkness on wet filter paper for 5-7 days at ambient temperature. This

492   experiment was done once.

493   Wild-type (isogenic) and phosphinothricin-resistant *Brassica juncea*[30] were

494   grown on soil under a 16-h-light/8-h-dark photoperiod with fluorescent light of 80 to 120

495   μmol photons m^{-2} s^{-1} at 22°C and 60% relative humidity. For senescence induction, fully

496   developed cotyledons were excised and incubated in permanent darkness on wet filter

497   paper for 5-7 d at ambient temperature.

498   Wild-type (isogenic) and phosphinothricin-resistant *Triticum aestivum*[31] were

499   grown on soil under a 16-h-light/8-h-dark photoperiod with fluorescent light of 80 to 120

500   μmol photons m^{-2} s^{-1} at 22°C and 60% relative humidity. For senescence induction,

501   leaves were excised and incubated in permanent darkness on wet filter paper for 5-7 d at

502   ambient temperature.

503

504   RNA Isolation and qRT-PCR

505   Total RNA was extracted using a Qiagen RNeasy Plant Mini Kit according to

506   manufacturer's instructions (DNase treatment was performed on-column). The

507   concentration and purity of RNA were determined by absorbance at 260/280 nm. First-

508   strand cDNA was synthesized from 1 μg of RNA using SuperScript III Reverse

509   Transcriptase with Oligo dT primers (Thermo Scientific). Reactions were run on a

510   QuantStudio 6 system machine (Thermo Scientific) using Sybr Green Master Mix

511   (Thermo Scientific) using primer listed in Supplementary Fig. 4 and Supplementary

512   Table 3. Gene expression values were calculated using Ct values and normalized using

513   the reference gene At1g13320[32].

514

515   **Metabolite extraction**

516   Arabidopsis and *Brassica napus* samples were collected in 2 mL Eppendorf tubes

517   containing 500 µL of 1.5 mm glass beads, weighted and snap-frozen in liquid nitrogen.

518   The frozen samples were ground using a MM300 Mixer Mill (Retsch) at 30 Hz for 5 min

519   and stored at -80°C until further processing. *Glycine max* samples were snap-frozen in

520   liquid nitrogen and ground with a mortar and pestle. Metabolites were extracted using 5-

521   10 (for leaf samples) or 10 -50 volumes (for seed samples; w/v) of ice-cold extraction

522   buffer (80% methanol, 20% water, 0.1% formic acid (v/v/v)). Extracts were homogenized

523   at 30 Hz for 5 min and centrifuged (14,000-16,000 g, 4°C). After re-centrifugation,

524   supernatants were transferred to LC vials and analyzed by LC-MS.

525

526   **LC-MS analysis of Arabidopsis T-DNA mutants, *Brassica juncea* and *Triticum***

527   ***aestivum* (untargeted metabolomics and relative quantification of acetyl-**

528   **aminoadipate and acetyl-tryptophan)**

529   The LC-MS instrument was composed of an Ultimate 3000 Rapid Separation LC

530   system (Thermo Scientific) coupled to a Bruker Compact ESI-Q-TOF (Bruker

531   Daltonics). The reverse-phase chromatography system consisted of an 150 mm C18

532   column (ACQUITY UPLC^{TM} BEH, 1.7 µm, 2.1 x 150 mm, Waters), which was

533   developed using LC-MS solvents (Chemie Brunschwig) with a gradient (flow rate of 0.3

534   mL min^{-1}) of solvent B (acetonitrile with 0.1% (v/v) formic acid) in solvent A (water with

535   0.1% (v/v) formic acid) as follows (all (v/v)): 5% for 0.5 min, 5% to 100% in 11.5 min,

536   100% for 4 min, 100% to 5% in 1 min and 5% for 1 min. Electrospray ionization (ESI)

537   source conditions were set as follows: gas temperature, 220°C; drying gas, 9 L min^{-1};

538   nebulizer, 2.2 BAR; capillary voltage, 4500 V; end plate offset, 500 V. Tuning conditions

539   were set as follows: funnel 1 RF, 250 Vpp; funnel 2 RF, 150 Vpp; isCID energy, 0 eV;

540   hexapole RF, 50 Vpp; quadrupole ion energy, 3.0 eV; quadrupole low mass, 90 m/z;

541   collision cell, 6 eV; pre-pulse storage time, 3 µs. The instrument was set to acquire over

542   the m/z range 50-1300, with an acquisition rate of 4 spectra s^{-1}. Conditions for MS^2 of

543   automatically selected precursors (data-dependent MS^2) were set as follows: threshold,

544   1000 counts; active smart exclusion (5x); active exclusion (exclude after 3 spectra,

545   release after 0.2 min, reconsider precursor if current intensity/previous intensity is ≥5);

546   number of precursors, 3; active stepping (basic mode, timing 50%-50%, collision RF

547   from 350 to 450 Vpp, transfer time from 65 to 80 µs, collision energy from 80 to 120%).

548   All data were recalibrated internally using pre-run injection of sodium formate (10 mM

549   sodium hydroxide in 0.2% formic acid, 49.8% water, 50% isopropanol (v/v/v)). After

550   data recalibration using DataAnalysis (version 4.2, Bruker Daltonics) and data conversion

551   to mzXML format using ProteoWizard MSConvert[33], metabolite features detected in Ws

552   and FLAG_076H05 (senescent leaves, four replicates) were aligned according to

553   retention time and relatively quantified using XCMS online[34] (pairwise comparison using

554   XCMS online pre-set parameters "UPLC/Bruker Q-TOF"). Up-regulated features in

555   FLAG_076H05 were identified at retention times of 2.8 min (labeled as "1" in Fig. 1a,

556   m/z 204.086 (fold change ≥10, p-value ≤0.005, intensity threshold 800,000)) and 6.5 min

557   (labeled as "2" in Fig. 1a, m/z 247.108 (fold change ≥10, p-value ≤0.005, intensity

558   threshold 100,000)) and further characterized as ions derived from N-acetyl-D/L-

559   aminoadipate and N-acetyl-D/L-tryptophan, respectively, by database searches in

560   METLIN[35] using MS and MS^2 spectra. Relative quantification of acetyl-aminoadipate

561   and acetyl-tryptophan in Arabidopsis mutants from different insertion mutant collections

562   was carried out by QuantAnalysis (version 2.2, Bruker Daltonics) using extracted ion

563   chromatogram (EIC) traces ([M+H]$^+$). Metabolomics data generated in this study have

564   been uploaded to the EBI MetaboLights database (http://www.ebi.ac.uk/metabolights/)

565   with the following accession number (MTBLS553).

566

567   **Absolute quantification of free amino acids in senescent leaves of Arabidopsis T-**

568   **DNA mutants**

569   The LC-MS instrument was composed of an Ultimate 3000 Rapid Separation LC system

570   (Thermo Scientific) coupled to a Q-Exactive mass spectrometer (Thermo Scientific). The

571   HILIC chromatography system consisted of SeQuant ZIC-pHILIC Polymeric column

572   (2.1 × 150 mm, 5 μM, EMD Millipore), which was developed using Optima™ LC/MS

573   solvents (Fisher Chemical) with a gradient (flow rate of 0.15 mL min^{-1}) of solvent B

574   (acetonitrile) in solvent A (20 mM ammonium carbonate, 0.1% ammonium hydroxide) as

575   follows (all (v/v)): 80% to 20% in 20 min, 80% to 20% in 0.5 min and 80% for 7.5 min.

576   The mass spectrometer was operated in full-scan (resolution, 70'0000; AGC

577   target, 1e6; Maximum IT, 20ms) polarity switch mode with the spray voltage set to +/-

578   3.0 kV, the heated capillary held at 275C, and the HESI probe held at 350C. Seventeen

579   labeled amino acids (MSK-A2-1.2, Cambridge Isotope Laboratories) were added to the

580   extraction solvent (80% methanol, 20% water) and used as internal standards. Standard

581   curves were performed for each 25 amino acids. Acetyl-aminoadipate was synthesized

582   using recombinant BAR as described below and all 24 other amino acids were purchased

583   from Sigma-Aldrich. Data analysis was performed with Xcalibur (Thermo Scientific).

584   Note that values for a few amino acids are shown as relative levels in Supplementary Fig.

585   2 because their concentrations in some samples were more than 10-fold higher than the

586   highest concentration of the standard.

587

588   **Absolute quantification of acetyl-aminoadipate and acetyl-tryptophan in seeds of**

589   **Arabidopsis T-DNA mutants and various tissues of *Glycine max* and *Brassica napus***

590   Metabolites were extracted as described above and then analyzed on an Ultimate

591   3000 Rapid Separation LC system (Thermo Scientific) coupled to a TSQ Quantum

592   Access MAX triple-quadrupole mass spectrometer (Thermo Scientific). The reverse-

593   phase chromatography system consisted of an 150 mm C18 column (Kinetex 2.6 µm

594   silica core shell C18 100Å pore, Phenomenex) which was developed using Optima™

595   LC/MS solvents (Fisher Chemical) with a gradient (flow rate of 0.6 mL min^{-1}) of solvent

596   B (acetonitrile with 0.1% (v/v) formic acid) in solvent A (water with 0.1% (v/v) formic

597   acid) as follows (all (v/v)): 2% for 3 min, 2% to 99% in 9 min, 99% for 4 min, 99% to

598   2% in 1 min and 2% for 1 min. The mass spectrometer was configured to perform two

599   selected-reaction-monitoring scans, each for 0.5 seconds, for acetyl-aminoadipate and

600   acetyl-tryptophan. The m/z resolution of Q1 was set to 0.4 FWHM, the nitrogen collision

601 gas pressure of Q2 was set to 1.5 mTorr, and the Q3 scan width was set to 0.500 m/z in

602 both cases. Selected reaction monitoring for acetyl-aminoadipate was as follows:

603 precursor ion selection at 204.086 m/z on positive ion mode, fragmentation at 10 V, and

604 product ion selection at 144.065 m/z. Selected reaction monitoring for acetyl-tryptophan

605 was as follows: precursor ion selection at 247.107 m/z on positive ion mode,

606 fragmentation at 20 V, and product ion selection at 188.070 m/z. Acetyl-aminoadipate

607 was synthesized using recombinant BAR as described below and used as standard. Pure

608 acetyl-tryptophan was purchased from Sigma-Aldrich.

609

610 **Heterologous expression of wild-type BAR and activity determination**

611 The BAR coding sequence was amplified by PCR (KaPa HiFi HotStart

612 polymerase; KaPa Biosystems) from genomic DNA extracted from homozygous plants of

613 the SAIL line SAIL_1165_B02 using primers SAIL_BAR_F_pPROEX and

614 SAIL_BAR_R_pPROEX (see Table S3) and then cloned into pProEX Hta (Invitrogen)

615 via *Eco*RI and *Hin*dIII resulting in a 6xHis-BAR fusion construct.

616 6xHis-tagged BAR protein was expressed in *E. coli* BL21(DE3) grown in Terrific

617 Broth medium. At an optical density at 600 nm of 0.6, protein expression was induced

618 with 1.0 mM IPTG and cells were grown at 37°C for 2.5 h. Cells from 1 L culture were

619 harvested by centrifugation and resuspended in 25 mL binding buffer (50 mM Tris-HCl

620 pH 8, 500 mM NaCl, 30 mM imidazole). All the following steps were carried out at 4°C.

621 Cell lysis was performed using a microfluidizer (HC-8000, Microfluidics). The lysate

622 was centrifuged (16,000 g) for 20 min, and the 6xHis-tagged BAR protein was purified

623 by metal affinity (5-ml HisTrap HP column, GE Healthcare) and size-exclusion

624 chromatography (HiLoad 16/600 Superdex 200 pg, GE Healthcare) using an ÄKTA Pure

625 FPLC system (GE Healthcare). The 6xHis-TEV tag was removed from BAR prior to

626 size-exclusion chromatography by overnight incubation with 1 μg of 6xHis-TEV

627 protease[36] per 10 μg protein in 50 mM Tris-HCl pH 8, 500 mM NaCl, 1 mM

628 dithiothreitol, followed passage through HisTrap HP column. Purified recombinant BAR

629 was dialyzed in storage buffer (12.5 mM Tris-HCl pH 8, 50 mM NaCl, 2 mM

630 dithiothreitol) and concentrated to 13 mg/mL using an ultra-centrifugal filter (10,000 Da

631 MWCO, Amicon EMD Millipore). The purity of recombinant BAR was assessed by

632 SDS-PAGE (Supplementary Fig. 6a). Purified BAR was aliquoted, snap-frozen in liquid

633 nitrogen and stored at -80°C until further use.

634   Enzyme assays were carried out in 2 mM Tris-HCl pH 8 and 10 mM acetyl-CoA

635 (Sigma-Aldrich; final volume 25 μl). Before determining the kinetics of BAR with

636 different substrates, time-dependent activity of the purified protein was tested at substrate

637 concentrations of 500 μM L-phosphinothricin (glufosinate ammonium, considered as a

638 1:1 mixture of L- and D- enantiomers; Sigma-Aldrich) or 1 mM (L-aminoadipate and L-

639 tryptophan; Sigma-Aldrich). Reactions were initiated by the addition of purified BAR at

640 0.26 μM (assays with L-phosphinothricin) or 150 μM (assays with aminoadipate or

641 tryptophan) and incubated at 25°C for the indicated times (Supplementary Fig.3 b-d).

642 Reactions were stopped by the addition of four volumes of 10% water, 90% acetonitrile

643 (v/v), 5 mM ammonium formate pH 3. Likewise, substrate concentration-dependence

644 was determined by incubating assays for 25 min (assays with L-phosphinothricin), 3 h

645 (assays with aminoadipate) or 7 h (assays with tryptophan; Fig. 3). Stock solutions of

646 aminoadipate and tryptophan at 60 mM were made in 2 mM Tris-HCl pH 8 supplemented

647   with 1 mM N-nonyl β-D-glucopyranoside and substrate concentration-dependence assays

648   employing these two substrates contained 0.33 mM N-nonyl β-D-glucopyranoside.

649   Control assays (Fig. 3) were performed with aminoadipate and tryptophan at 20 mM, but

650   in the absence of BAR.

651   The assays were analyzed on an Ultimate 3000 Rapid Separation LC system

652   (Thermo Scientific) coupled to a TSQ Quantum Access MAX triple-quadrupole mass

653   spectrometer (Thermo Scientific). Assays on phosphinothricin were analyzed as follows.

654   The normal-phase chromatography system consisted of an 150 mm HILIC column

655   (Kinetex 2.6 μm silica core shell HILIC 100Å pore, Phenomenex), which was developed

656   using Optima™ LC/MS solvents (Fisher Chemical) with a gradient (flow rate of 0.8 mL

657   min^{-1}) of solvent B (50% water, 50% acetonitrile (v/v), 5 mM ammonium formate pH 3)

658   in solvent A (10% water, 90% acetonitrile (v/v), 5 mM ammonium formate pH 3) as

659   follows (all (v/v)): 0% for 2 min, 0% to 70% in 10 min, 70% to 100% in 30 sec, 100% for

660   90 sec, 100% to 0% in 30 sec and 0% for 3.5 min. The mass spectrometer was configured

661   to perform selected-ion-monitoring scans of 0.5 seconds using Q3 (center mass m/z:

662   224.068, scan width 1.0 m/z, scan time 0.5 sec). Assays on aminoadipate and tryptophan

663   were analyzed as described above for the absolute quantification of acetyl-aminoadipate

664   and acetyl-tryptophan in planta. Product formation was quantified using standards

665   synthesized using recombinant BAR (acetyl-phosphinothricin and acetyl-aminoadipate)

666   or commercially available (acetyl-tryptophan, Sigma-Aldrich). K_m and V_{max} value for

667   phosphinothricin were inferred using the Michaelis-Menten kinetics nonlinear regression

668   function under Prism 6 (GraphPad).

669

X-ray crystallography

670

671 Purified BAR protein was incubated with 1 mM acetyl-CoA for >2 hour prior to

672 setting crystal trays. Crystals of BAR were obtained after 3 days at 20 °C in hanging

673 drops containing 1 μL of protein solution (7.5 mg/mL) and 1 μL of reservoir solution

674 (0.18 M calcium acetate, 0.1 M Tris-HCl pH 7, 18% (w/v) PEG 3000, 0.2% (v/v) N-

675 nonyl β-D-glucopyranoside, 1 mM acetyl-CoA). Several crystals were soaked in reservoir

676 solution supplemented with 30 mM L-phosphinothricin for 30-60 min before freezing.

677 Crystals were frozen in reservoir solution supplemented with 15% (v/v) ethylene glycol.

678 Acetylation of phosphinothricin occurred during soaking as no density for the acetyl

679 group of acetyl-CoA was observed in the BAR/CoA/phosphinothricin ternary complex.

680 X-ray diffraction data were collected on the 24-ID-C beam line of the Structural

681 Biology Center at the Advanced Photon Source (Argonne National Laboratory) equipped

682 with a Pixel Array Detector (Pilatus-6MF). Diffraction intensities were indexed,

683 integrated, and scaled with the iMosflm[37] and SCALA[38] programs. Initial phases were

684 determined by molecular replacement using Phaser under Phenix[39]. The search model

685 was an ensemble model generated with Ensembler using 8 protein structures homologous

686 to BAR (PBD codes and % identity to BAR: 2JLM (28%), 3DR8 (35%), 4J3G (31%),

687 4JXQ (33%), 4MBU (30%), 1VHS (30%), 1YR0 (29%) and 1YVO (35%)). Subsequent

688 structural building and refinements utilized Phenix programs (TSL was used in early

689 rounds of refinement)[39]. Coot was used for graphical map inspection and manual

690 rebuilding of atomic models[40]. Crystallographic calculations were performed using

691 Phenix. Molecular graphics were produced with the program PyMol.

692

Heterologous expression of BAR mutants and activity determination

Single amino acid mutants of BAR were generated using the QuikChange II site-directed mutagenesis kit (Agilent Technologies) and 6xHis-BAR in pProEX Hta as template (see Supplementary Table 3 for primer sequences). PAT from *Streptomyces viridochromogenes* was amplified using primers BAC0327 and BAC0328 from pAG31 vector [41] (Addgene 35124) and cloned into *Bam*HI/*Hin*dIII-linearized pProEX Hta by Gibson assembly (New England Biolabs). Wild-type 6xHis-BAR, 6xHis-BAR mutants and 6xHis-PAT were expressed in *E. coli* BL21(DE3) grown in Terrific Broth medium. At an optical density at 600 nm of 0.6, protein expression was induced with 1.0 mM IPTG and cells were grown at 37°C for 2.5 h. Cells from a 150 mL cultures were harvested by centrifugation, lysed using B-PER™ Bacterial Protein Extraction Reagent (Thermo Scientific) and purified by metal affinity using Ni-NTA Agarose (Qiagen). Purified recombinant proteins were concentrated and buffer-exchanged using storage buffer (10 mM Tris-HCl pH 8.0, 0.2 M NaCl, 10% (v/v) glycerol, 1 mM dithiothreitol) and ultra-centrifugal filters (10,000 Da MWCO, Amicon EMD Millipore). The purity of the recombinant proteins was assessed by SDS-PAGE. Final protein concentrations were determined and normalized using a NanoDrop 2000 UV-VIS spectrometer (extinction coefficient: 43430 M^{-1} cm^{-1}, Thermo Scientific).

Enzyme assays for comparing the relative activity of the purified BAR mutants were carried out in 2 mM Tris-HCl pH 8 and 5 mM acetyl-CoA (Sigma-Aldrich) (final reaction volume 12 µL). Reactions were initiated by the addition of purified recombinant protein at 0.2 µM (assays with L-phosphinothricin at 0.2 mM) or 150 µM (assays with aminoadipate or tryptophan at 1 mM) and incubated at 25°C for 15 min

716　(phosphinothricin), 165 min (aminoadipate), or 330 min (L-tryptophan). Substrate

717　concentration-dependences toward phosphinothricin, aminoadipate and tryptophan were

718　determined for the BAR mutants Y92F and N35T in 2 mM Tris-HCl pH 8 and 10 mM

719　acetyl-CoA (Sigma-Aldrich). Note that assays on aminoadipate and tryptophan were

720　supplemented with 0.33 mM of N-nonyl β-D-glucopyranoside (see also above).

721　Reactions were stopped by the addition of four volumes of 10% water, 90% acetonitrile

722　(v/v), 5 mM ammonium formate pH 3, centrifuged for 2 min (14,000-16,000 g), and

723　transferred to LC vials.

724　　　The assays were analyzed on an Ultimate 3000 Rapid Separation LC system

725　(Thermo Scientific) coupled to a TSQ Quantum Access MAX triple-quadrupole mass

726　spectrometer (Thermo Scientific). Assays on phosphinothricin were analyzed as

727　described above. Assays on aminoadipate were analyzed as follows. The reverse-phase

728　chromatography system consisted of an 150 mm C18 column (Kinetex 2.6 μm silica core

729　shell C18 100Å pore, Phenomenex), which was developed using Optima™ LC/MS

730　solvents (Fisher Chemical) with a gradient (flow rate of 0.6 mL min^{-1}) of solvent B

731　(acetonitrile with 0.1% (v/v) formic acid) in solvent A (water with 0.1% (v/v) formic

732　acid) as follows (all v/v): 1% for 2 min, 1% to 30% in 9 min, 30% to 99% in 30 sec, 99%

733　for 30 sec, 99% to 1% in 1 min and 1% for 2 min. The mass spectrometer was configured

734　to perform selected-ion-monitoring scans of 0.5 seconds using Q3 (center mass m/z:

735　204.086, scan width 0.5 m/z, scan time 0.5 sec). Assays on tryptophan were analyzed as

736　follow: the reverse-phase chromatography system consisted of an 150 mm C18 column

737　(Kinetex 2.6 μm silica core shell C18 100Å pore, Phenomenex) which was developed

738　using Optima™ LC/MS solvents (Fisher Chemical) with a gradient (flow rate of 0.7 mL

739   min^{-1}) of solvent B (acetonitrile with 0.1% (v/v) formic acid) in solvent A (water with

740   0.1% (v/v) formic acid) as follows (all v/v): 5% for 1 min, 5% to 99% in 9 min, 99% for

741   2 min, 99% to 5% in 2 min and 5% for 1 min. The mass spectrometer was configured to

742   perform selected-ion-monitoring scans of 0.5 seconds using Q3 (center mass m/z:

743   247.108, scan width 0.5 m/z, scan time 0.5 sec).

744

Analysis of BAR mutants in planta

746   Wild-type BAR from *Streptomyces hygroscopicus*, selected BAR mutants and wild-type

747   PAT from *Streptomyces viridochromogenes* were amplified by PCR (Phusion

748   polymerase; New England Biolabs) from pProEX Hta clones (see above) using primers

749   listed in Table S3 and cloned into *Bpi*I-linearized pICH41308[42] (Golden Gate entry

750   vector) by Gibson assembly (New England Biolabs). BAR and PAT coding sequences

751   were fused with *Agrobacterium tumefaciens* mannopine synthase promoter (from

752   pICH85281) and terminator (from pICH77901) into the empty binary vector pICH47732

753   by Golden Gate assembly[42]. pICH47732 constructs were transformed into *Agrobacterium*

754   *tumefaciens* GV3130 strain by electroporation and transformed into Arabidopsis Col-0 by

755   the floral dip method [43]. 90 mg of T1 seeds were sown on soil and transformants were

756   selected with Finale® (contains 11.33% glufosinate ammonium; Bayer CropScience)

757   diluted 1:500 in water. Photographs were taken 10 days after herbicide treatment (**Fig. 4**

758   and **Supplementary Fig. 12**). This experiment was repeated once with similar results. T2

759   seeds from 5 to 6 T1 plants were collected for each BAR mutants, sown on soil and

760   transgenic individuals were selected with Finale® (contains 11.33% glufosinate

761   ammonium; Bayer CropScience) diluted 1:500 in water (**Supplementary Fig. 13**). This

762   experiment was done once. Metabolites were extracted from dark-incubated leaves

763   collected from T2 phosphinothricin-resistant individuals (senescent leaves from 8-9

764   individuals were pooled for each T2 population) and then analyzed as described above

765   for the absolute quantification of acetyl-aminoadipate and acetyl-tryptophan in *Glycine*

766   *max* and *Brassica napus.*

767   To further compare the phosphinothricin tolerance in T2 lines transformed with

768   Y92F, N35T and wild-type BAR, seeds from 5-6 independent lines were germinated on

769   ½ MS medium containing 1% sucrose and 8 μg/mL glufosinate ammonium (45520-

770   Sigma-Aldrich). Seven-days old seedlings were then transformed on soil and further

771   grown for 10 days. Photographs were taken before treatment with four different

772   concentrations of Finale® (0, 0.2X, 1X and 5X; see **Supplementary Fig. 14** for further

773   details on the herbicide concentrations). Plants were further grown for 8 days,

774   photographs were taken and the average aerial mass of each T2 populations was

775   measured (average from 8-9 individuals). This experiment was done once.

776   Protein levels of the BAR mutants in T2 lines were measured as follow. For each

777   protein extraction, equal amounts of aerial tissues from 5-6 transgenic T2 populations

778   were pooled. Total proteins were isolated from frozen samples by homogenization in 5

779   volumes of ice-cold extraction buffer [50 mM Tris–HCl pH 8, 100 mM NaCl, 0.5% (v/v)

780   TritonX-100, 2mM β-mercaptoethanol] complemented with a protease inhibitor cocktail

781   (Complete; Roche Diagnostics). Samples were centrifuged at 12,000 g for 5 min and

782   protein concentration of the supernatant was determined using the Bradford Assay (Bio-

783   Rad). Proteins were subsequently precipitated with chloroform–methanol and 10 μg were

784   analyzed by SDS-PAGE and immunoblotting as described [44]. The following antibodies

785 were used for immunoblot analysis: a primary polyclonal antibody against BAR from

786 *Streptomyces hygroscopicus* produced in rabbit (1:1000; P0374-Sigma-Aldrich) and a

787 polyclonal horseradish peroxidase conjugated goat anti-rabbit IgG as the secondary

788 antibody (1:50000; A0545-Sigma-Aldrich). Substrate detection was performed by

789 chemiluminescence (ECL Western Blotting Substrate™ (Pierce)) and film exposure. This

790 experiment was done once.

791

792 **Data availability**

793 The data that support the findings of this study are available from the corresponding

794 authors upon reasonable request.
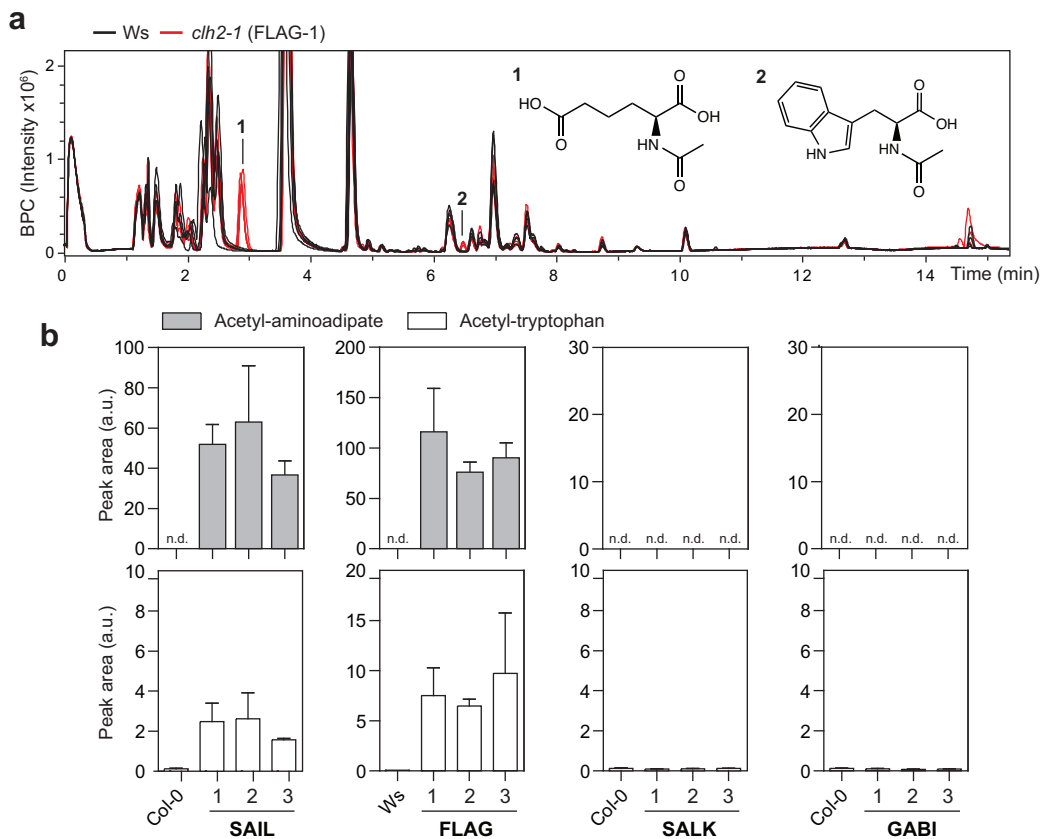
Figure 1 | Accumulation of acetyl-aminoadipate and acetyl-tryptophan in senescent leaves of Arabidopsis carrying the BAR transgene. a, Metabolite profiles of senescent leaves from Wassilewskija (Ws) and *clh2-1* (FLAG-1), displayed as base peak chromatograms (BPC), reveal the ectopic accumulation of acetyl-aminoadipate ('1') and acetyl-tryptophan ('2'). BPC traces of four biological replicates are displayed. **b**, Comparative levels of acetyl-aminoadipate and acetyl-tryptophan in Arabidopsis mutants from different insertional mutant collections that contain either BAR (SAIL and FLAG) or alternative selection marker genes (SALK (*NTPII*, kanamycin resistance) and GABI (*SULI*, sulfadiazine resistance)). Error bars, mean ± s.d. (n = 3 biological replicates). This experiment was repeated at least three times with similar results. See Supplementary Figure 2 for absolute quantification. a.u., arbitrary unit; FW, fresh weight; n.d., not detected
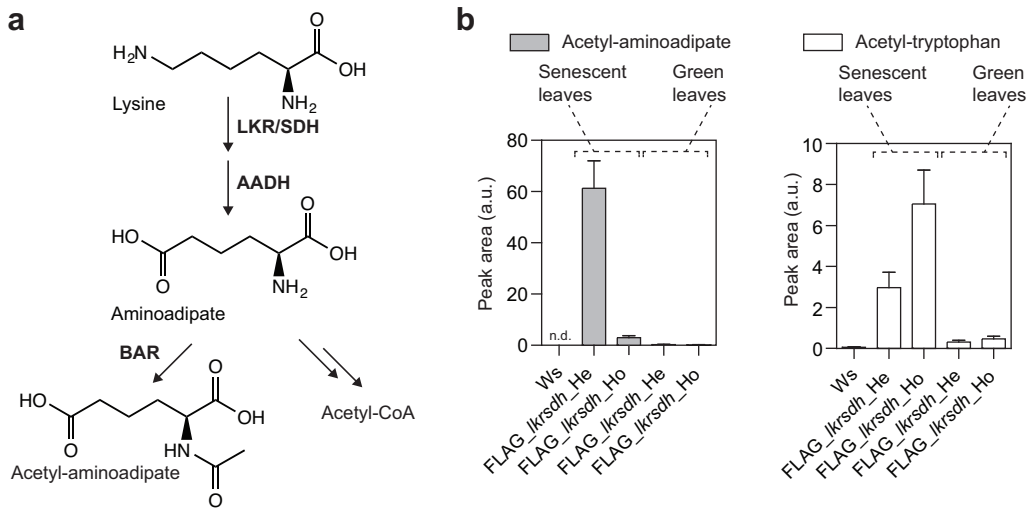
Figure 2 | BAR-dependent accumulation of acetyl-aminoadipate and acetyl-tryptophan is linked to nitrogen remobilization during senescence. a, Aminoadipate is derived from the lysine degradation pathway in plants, which can be metabolized by BAR as a nonspecific substrate. **b**, Comparative levels of acetyl-aminoadipate and acetyl-tryptophan in green and senescent leaves from the heterozygous (He) and homozygous (Ho) FLAG_*lkrsdh* mutant, harboring a BAR-containing T-DNA that abolishes the Arabidopsis *LKR/SDH* gene. Error bars, mean ± s.d. (n = 4 biological replicates). a.u., arbitrary unit; n.d., not detected; Ws, Wassilewskija wild-type plants.
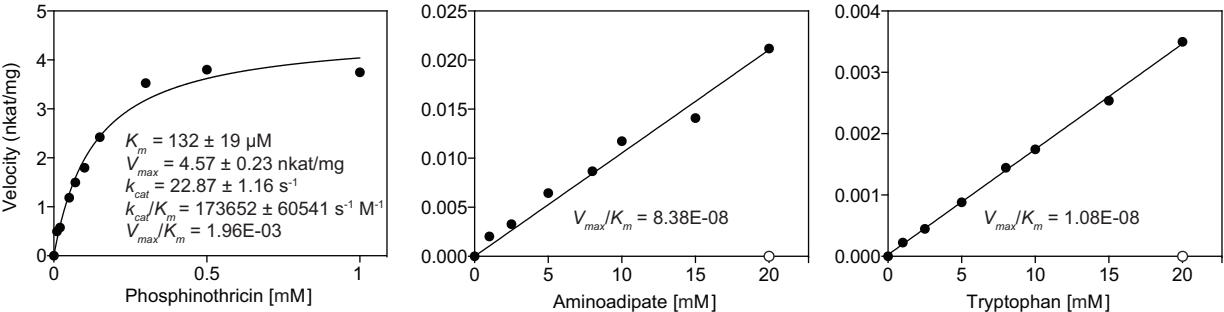
Figure 3 | *In vitro* enzyme kinetic assays of BAR against native and non-native substrates. An apparent K_M value of 132±19.2 µM was obtained for phosphinothricin, similar to previously published data[1, 3, 17]. V_{max}, k_{cat}, k_{cat}/K_m and V_{max}/K_m values for phosphinothricin are also indicated, as well V_{max}/K_m values for aminoadipate and tryptophan (estimated from Lineweaver-Burk plots). Aminoadipate and tryptophan are *in vitro* substrates of BAR but both substrates reached solubility limit before reaching saturation concentration for BAR. Negative controls (open circles) were performed in absence of BAR at the highest substrate concentration tested (20 mM).
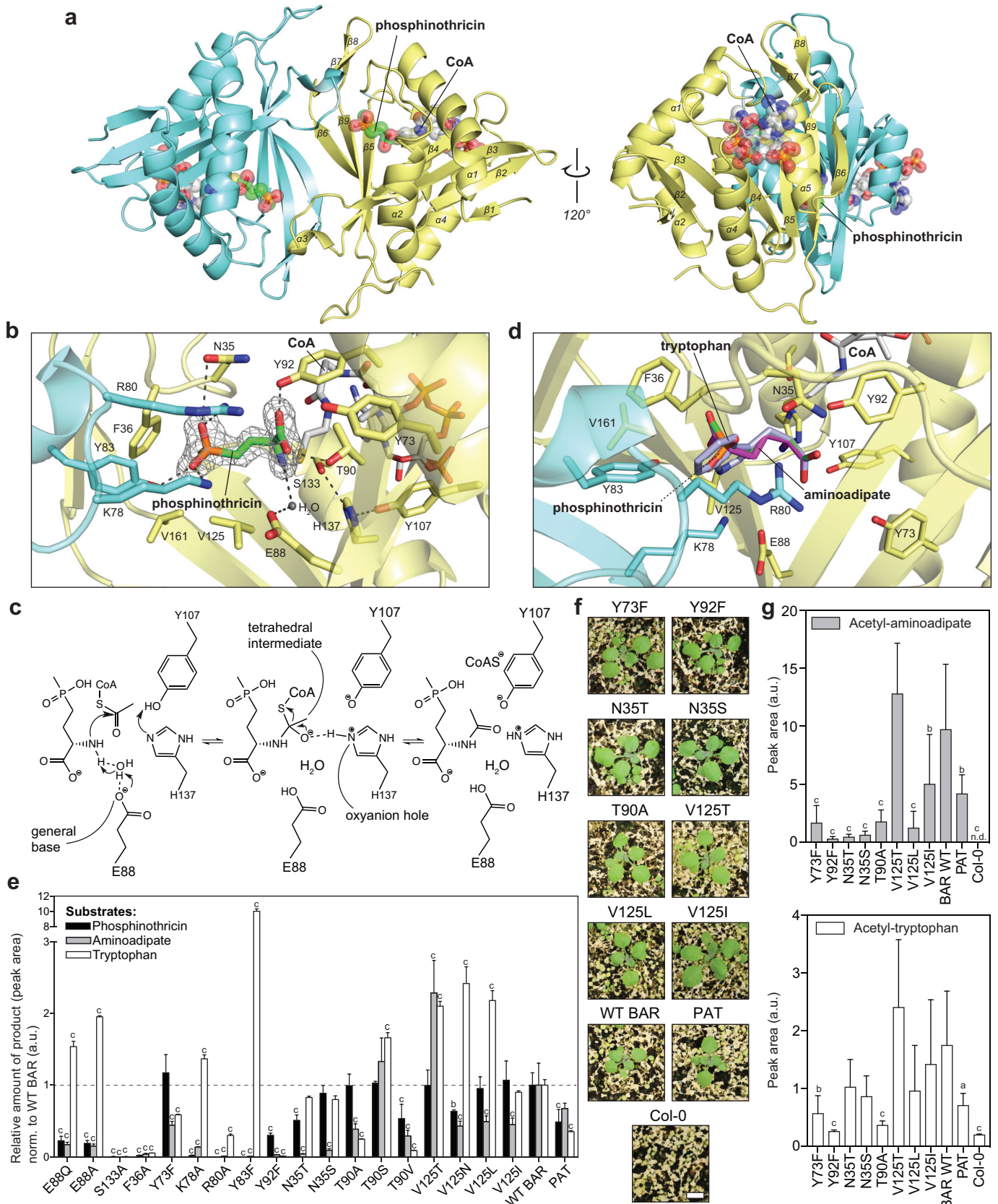
Figure 4 | Structural basis for amino acid N-acetylation catalyzed by BAR and structure-guided engineering of BAR with reduced nonspecific activities. a, Cartoon representation of BAR homodimer in complex with phosphinothricin and CoA. Two monomers of the dimer are colored in blue and yellow respectively. **b**, Close-up view of the BAR active site. The |2Fo-Fc| omit electron density map (contoured at 3.0 σ) is shown for phosphinothricin. **c**, Proposed catalytic mechanism of BAR. **d**, Docking of tryptophan and aminoadipate within the BAR active site reveals reduced favorable contacts compared to phosphinothricin. **e**, Enzyme activity assays using purified BAR mutant proteins against phosphinothricin (0.2 mM), aminoadipate (1 mM) and tryptophan (1 mM). Wild-type BAR (WT BAR) and PAT from *Streptomyces viridochromogenes* were also examined as controls. Assays were terminated during the initial linear rate of product formation. The relative amount of product formed by each BAR mutant was normalized to WT BAR for each substrate (value of 1). Error bars, mean ± s.d. (n = 3 technical replicates). **f**, Photographs of Arabidopsis T1 lines transformed with select BAR mutants 10 days after phosphinothricin treatment (see also Supplementary Fig. 12, 13 and 14). Scale bar = 0.3 cm. **g**, Comparative levels of acetyl-aminoadipate and acetyl-tryptophan in phosphinothricin-resistant T2 Arabidopsis plants transformed with selected BAR mutants. Error bars, mean ± s.d. (n = 5-6 biological replicates (Y73F (6), Y92F (6), N35T (5), N35S (5), T90A (6), V125T (5), V125L (6), V125I (6), WT BAR (5), PAT (5)). Significance levels were indicated based on one-way ANOVA with Dunnett's test for multiple comparisons to WT BAR. a, p-value<0.1; b, p-value<0.05; c, p-value<0.01; a.u., arbitrary unit.